Proceedings World Geothermal Congress 2020+1
Reykjavik, Iceland, April - October 2021

Integrated Analysis of Gravity-gradient and Geomagnetic Survey Data in Geothermal Prospective Area in Japan

Shigeki Mizutani

Kawasaki Geological Engineering Co., Ltd, 2-11-15 Mita, Minato-ku, Tokyo, 108-8337 Japan

mizutanis@kge.co.jp

Keywords: gravity gradient, aero-magnetic, integrated analysis

ABSTRACT

Poisson's theorem describes the relation existing between gravitational and geo-magnetic potentials. The integrated analysis of surface gravity and aero-magnetic datasets is adequate to calculate subsurface magnetization-to-density ratio by converting aero-magnetic data to those of pseudo-gravity data and repeatedly applying the theorem within a small, moving data window. The results show the regional variation of the ratio, and lead to delineate not only appeared to surface but buried volcanic conduits and intrusive rocks, and to estimate an approximate age of volcanic activities. These delineation trends are considered as being along possible deep strike-slip faults, which are normally oriented along the NW-SE. The analysis is extended to the application for the gravity-gradient and magnetic datasets, which are acquired by helicopter at low flight height and with extremely dense measurement density in the mountainous areas where several geothermal prospects are located, in the south-eastern part of Akita prefecture, Japan. The magnetic data are converted to those of reduction to pole. The grid interval can be 25 m. The correlations between the two datasets are extremely well. The results of analysis show the detailed variations of mainly near-surface (up to about 500m from surface) magnetization-to-density ratio. These help to assess not only the precise near-surface distribution of volcanic conduits and intrusive rocks, but the possible extension of near-surface lava distributions. the delineation of possible strike-slip faults more in details and the local stress distributions under the regional E-W compressional field. The geological information obtained by the analysis helps to interpret the distributions of heat sources and releasing type fractures, and consequently contributes to evaluate geothermal potentials more accurately.

1. INTRODUCTION

Geothermal fluid is produced from rain-fall water which penetrates in undergrounds through areas of high permeable rocks such as fractured areas, is heated by high temperature rocks such as magma, intrusive rocks etc., and is sometimes mixed with high temperature magmatic water and extruded minerals from hydrothermally altered rocks. A part of geothermal fluid mainly consisted of high temperature hot water and vapor is kept in high permeable geothermal reservoirs, and the remaining will discharge out on the ground at hot springs and fumaroles etc. These subsurface passes of geothermal water in the past can also be traced by surface and subsurface hydrothermal alteration zones.

It is essentially important to evaluate geologically this subsurface geo-circulation system of geothermal fluid by assessing the locations of areas of rain-fall water's penetration in underground, subsurface high permeable layers, heat sources, geothermal reservoirs etc. The preceding stage of the system; the areas of water's penetration can be properly estimated by the application of the Horizontal Gravity Gradient Stack (HGGS) analysis for the airborne gravity-gradient data proposed by Mizutani (2018). The precise density variations of surface-layer can be obtained. Consequently, the areas where rocks with high permeability distribute such as un-consolidated layers, high porosity layers etc. can be estimated.

The main stages of the system; subsurface locations of heat sources and reservoirs are deeply related with those activities and behaviors of magma and geothermal fluid. The hydrothermal processes are associated with swellings of extracted ashes and clays, and therefore tend to occlude geothermal reservoirs by those clays and ashes which fill in and block the porous parts of the rocks. The sustainable formation of geothermal reservoirs needs geological stress fields which mitigate and prevent the occlusion. Under the geologically compressional stress fields, the expansional stresses occur toward the orthogonal direction of compressional stresses and contribute to the formation of releasing type of fractures, which will act as the sustainable geothermal reservoirs.

The geothermal fluid as well as magma tends to intrude in the openings of the fractures and faults made by the expansional stresses. As the intruded magma cools down, it becomes intrusive rocks and obtains the remnant magnetization. Accordingly, the distributions of magma and intrusive rocks are closely related to those of heat sources and reservoirs of geothermal resources.

This paper deals with a method of upgrading the evaluation of geothermal resources. It explains an integrated analysis, applying Poisson's theorem of gravity-gradient and geo-magnetic data sets which are acquired with high spatial density.

2. GEOLOGICAL MODEL

2.1 Geologically Compressional Stress Fields

Figure 1 shows an interpreted reflection seismic section (left) and its schematic geological section (right) acquired in Akinomiya area, a geothermal potential region situated in north-east Japan. The location of the line is shown in the left map of Figure 5.

Mizutani (2012) explained that series of faults can be observed in the seismic section. Each stem of fault originates from and cuts deeply seated horizontal intrusive rocks. Each fault develops the flower structures in its shallow part, and some faults reach near to the surface. This implies that their formation was made under geologically compressional stress fields. Homogeneous patterns of

reflection waves are observed along these faults. This suggests that large volume of hot water passed through the faults and the hydrothermal alterations occur in the rocks along these faults as illustrated in the left drawing of Figure 2. They become altered to relatively simple minerals. The hydrothermal alteration becomes weaker as it gets farther apart from the faults and forms a layered structure of altered materials. In addition, it is observed that the homogenous pattern along the faults diminishes in the upper part of the faults. This suggests that scales are produced by reduction of temperature and pressure in addition to the swellings of extracted clays and ashes. These scales, clays and ashes occluding the porous part of fractures and faults will act possibly as cap rock.

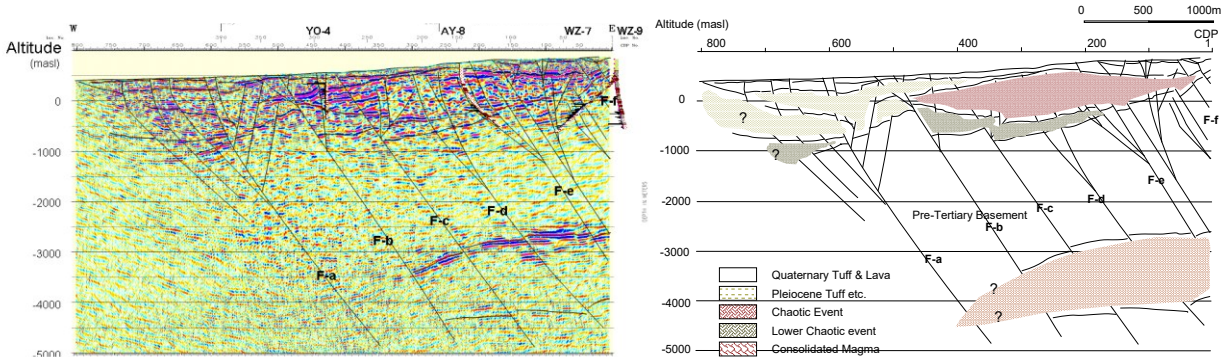

Figure 1: Interpreted reflection seismic section (left) and its schematic geological section (right).

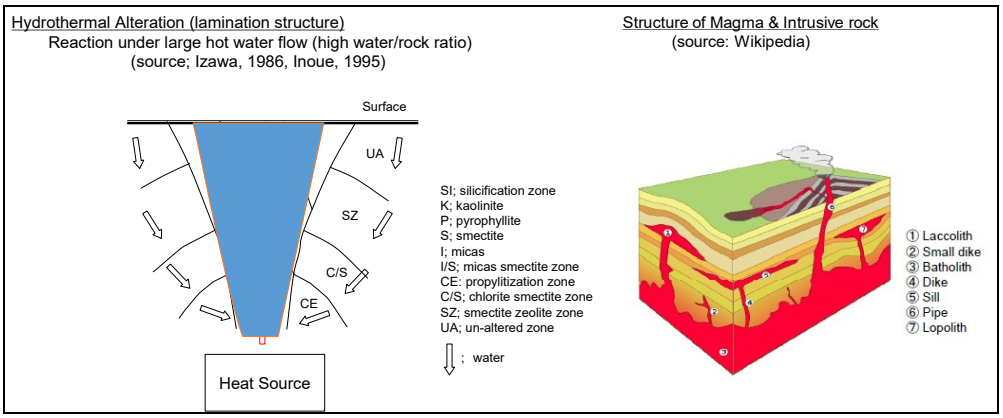

Figure 2: Laminated structure of hydrothermal alteration (left) and structure of magma (right).

Figure 3 shows a model of structure formation under compressional stress fields. The drawings (a), (b) and (c) are presented by Hancock (1994) and modified by Taira (2001). The drawing (a) illustrates the schematic formation of structures which is developed under compressional stress fields. The pull apart basin develops along the strike-slip fault. The drawing (b) and (c) shows two types of flower structures at upper parts of the stem. The (b) is associated with zones of trans-pression of the strike-slip fault, while the (c) associated with zones of trans-tension. The drawing (d) shows that the expansional stresses occur toward the orthogonal direction of compressional stresses and form normal faults. The drawing (e) shows that the extensional bend to be formed by the movement of strike-slip faults acts as openings (as shown in red circle) of fractures and faults where magma as well as geothermal fluid intrudes. These faults shown in the drawings (c), (d) and (e) can form releasing type of fractures and act possibly as sustainable reservoirs if geothermal fluid intrudes in.

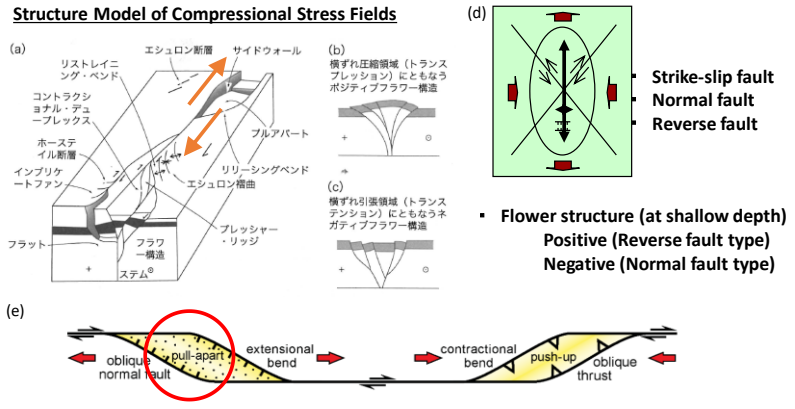

Figure 3: Model of structure formation under compressional stress fields

2.2 Intrusive Rocks and Remnant Magnetization

The right drawing of Figure 2 shows a schematic drawing of magma intrusion in the volcanic area. As for vertical intrusion, dike, small dike and pipe are illustrated. As for horizontal intrusion, sill, laccolith, lopolith etc. are illustrated.

When the openings of the fractures and faults are made by the expansional stresses, the geothermal fluid as well as magma tends to intrude in the openings. Accordingly, the distributions of geothermal reservoirs (which may not always contain geothermal fluid but remaining of hydrothermal alteration), magma and intrusive rocks tend to scatter along the common normal faults and openings formed along the strike-slip faults. As the intruded magma cools down, it becomes intrusive rocks and obtains the remnant magnetization. Therefore, it becomes possible to assess such linear distribution of geo-magnetic responses as caused by magma and intrusive rocks.

In addition to the vertical intrusions of magma in terms of estimating the distribution of geothermal reservoirs, it is important to assess the subsurface locations of the horizontal intrusions such as laccolith etc. To understand their relations with the compressional stress fields will help assess the distributions of and factors forming to geothermal reservoirs and heat sources.

3. ANALYSIS

3.1 Poisson's Theorem

Poisson (1826) shows the relationship between gravitational and magnetic potentials (as defined, "Up" and "Vp", respectively) arising from a common, isolated uniform source. The relationship is independent of the shape and position of the source.

Chandler et al. (1981) state that the application of Poisson's theorem is useful in combined analysis of gravity and magnetic anomaly data sets, and propose its application using the modified expression of the relationship between the total field magnetic intensity anomaly reduced to the pole (as defined in this paper, "RTPM") and the vertical gravity-gradient anomaly (as defined in this paper, "G_{zz}"). The relationship as modified in SI unit is formulated as follows;

$$RTPM=(\mu_0/4\pi)(1/G)(J/\rho) \times G_{zz} + A \quad (1)$$

where μ_0, G, J and ρ are vacuum magnetic permeability ($4\pi \times 10^{-7} NA^{-2}$), universal gravitational constant ($6.67384 \times 10^{-11} m^3 kg^{-1} s^{-2}$), magnetization (in A/m) and density (in kg/m^3), respectively. A is approximately constant and accounts for base level change caused by long-wavelength anomaly component.

Mizutani (2016) shows that its application using the farther modified expression of the relationship between the gravity (as defined in this paper, "BG") and pseudo-gravity (as defined in this paper, "PsG") is also useful in determining magnetization-to-density ratio in geothermal resources potential regions in Japan. The results, although with coarse grid interval of 500m due to acquisition constraint, show satisfactorily the regional variation of the ratio, and lead to delineate not only appeared to surface but buried volcanic conduits and intrusive rocks, and to estimate an approximate age of volcanic activities. These delineation trends are considered as being along possible deep strike-slip faults.

3.2 Moving Window Poisson's Analysis

Chandler et al. (1981) and Mizutani (2016) explain how a moving window Poisson's analysis works. A small window is selected around a certain grid (x_0, y_0). A pair of the RTPM(x, y) and the G_{zz}(x, y) at each grid (x, y) fallen in the window is selected, and plotted as the value of RTPM on y-axis and the value of G_{zz} on x-axis. Base on the equation (1), a linear distribution of these plot will be expected if the variations of J(x, y) and ρ(x, y) are gentle. The slope of the linear distribution corresponds to a value of $(\mu_0/4\pi)(1/G)(J/\rho)$ at grid (x_0, y_0). Consequently, the value of J/ρ at the grid (x_0, y_0) is obtained.

The above calculation will be made at the adjacent grid using the same window size, and the value of J/ρ at such adjacent grid will be obtained. This calculation will be repeatedly applied and expanded in the entire studied area, and the distribution of J/ρ(x, y) will be obtained.

3.3 Characteristic of data sets of RTPM and G_{zz}

3.3.1 Data of RTPM and G_{zz}

JOGMEC (2014) and Mizutani (2018) explaine that the gravity-gradient is a tensor of 9 components out of which 5 are independent. The acquired data in this study are 2 horizontal gravity-gradient components, namely in this paper G_{xy} and G_{uv}. A single source response of G_{uv} has a distribution pattern of 45-degree anti-clockwise rotation of that of G_{xy}. The data of vertical gravity-gradient (G_{zz}) can be calculated using acquired data of both G_{xy} and G_{uv} through the 2D Fourier transformation.

The RTPM is calculated from the acquired total field magnetic intensity anomaly data with the assumption of the average geomagnetic inclination and declination of the studied area.

The distribution pattern of a single source response of both RTPM and G_{zz} has a similar shape. The responses of both RTPM and G_{zz} from a respective single source magnetization or mass (density) are proportional to the third power of the reciprocal value of a distance between a measuring point and a point source.

3.3.2 Peak amplitude of a single source response

The wavenumber analysis of a single source response shows that the peak spectrum is observed at the wavelength of about 6 to 7 times of average flight height of the survey and that the amplitude of spectrum declines as the wavelength becomes longer or shorter than that of peak. There is no response at wavelength of infinity, and therefore no response of RTPM or G_{zz} arose from

subsurface layers whose respective magnetization or density is constant. If a depth of a single source becomes deeper, then overall amplitudes of spectrum become smaller and the wavelength where the peak spectrum is observed becomes longer.

3.3.3 Explorable Depth

The observed data of both RTPM and G_{zz} have larger effects from the respective variation of magnetization or mass (density) of shallower subsurface layers than those of deeper. Consequently, the explorable depth by both surveys is shallow and limited. Based on the analysis of observation data mentioned later, it may be about 600 m from the measuring plane if the average flight height is 150 m, implying the explorable depth of about 4 times of the average flight height. It depends on the noise level of the survey.

3.3.4 Surface Effects

Both gravity-gradient and geomagnetic data sets used in this study are acquired by helicopter. In order to acquire the data of high resolution, the flight height is kept rather low, about 150m. The geothermal resources potential regions are located generally in the mountainous areas, and the constant flight height cannot be kept during the survey.

As for the gravity-gradient survey, the responses of the surface roughness or the variation of flight height are not straightforward and cannot be neglected if the data are not acquired at the constant flight height. Mizutani (2018) shows that if high-density layers sit on convex ridge and low-density layers deposit at concave surface (normal case), its gravity-gradient response is the one responding as if the density of surface-layer is larger than that of matrix. On the contrary, if low-density layers sit on convex ridge and high-density layers deposit at concave surface (reverse case), its gravity-gradient response is the one as if the density of surface-layer is smaller than that of matrix. Therefore, it is not always positive response from convex ridge and negative response from concave, depending on the value of density at convex or concave relative to that of matrix.

As for the geomagnetic survey, the same analysis will apply as the above, however the cases of thin lava on the convex ridge and lava deposit at concave will be satisfactory to be considered. The surface effects are small and negligible compared with those of geomagnetic effects from underlying layers in the areas of vertical intrusion and massive horizontal intrusions. As the magnetizations of tuff and basement rocks are negligible compared with that of intrusive rocks, “0” magnetization is to be corresponding to the matrix density while positive magnetization as high-density and negative as low-density as simulating the case of analysis of gravity-gradient. In short, the surface effects need to be considered where the small magnetization or small absolute value of $\Delta J/\Delta\rho$ ratio is observed.

3.3.4 $\Delta J/\Delta\rho$ ratio

The $\Delta J/\Delta\rho$ is used in the following explanation replacing the J/ρ.

The relationship applied of Poisson’s theorem is independent of the shape and position of the source. Therefore, the $\Delta J/\Delta\rho$ ratio is considered as the (shallower depth weighted) average magnetization-to-density ratio from the surface down to the explorable depth. It represents basically the variation of the moving-average magnetization because the variation of $\Delta\rho$ ratio is gentle and rather constant compared with the tendency of abrupt change of ΔJ.

For the areas where vertical intrusive rocks are underlain, the large absolute values of $\Delta J/\Delta\rho$ ratio are expected. For the areas free from geomagnetic influences situated far away from volcanic areas, the small absolute values of $\Delta J/\Delta\rho$ are expected. For the areas where horizontal intrusive rocks are underlain or lava deposits, the absolute values of $\Delta J/\Delta\rho$ ratio will be expected in between.

The positive $\Delta J/\Delta\rho$ ratio will be expected if there are recent intrusive rocks, lavas etc. The negative $\Delta J/\Delta\rho$ ratio indicates that the intrusive rocks and lavas etc. are dated older than in Matsuyama period while the zero indicates probably the presence of magma. Considering the surface effects mentioned above, the $\Delta J/\Delta\rho$ ratio become random where the effects from intrusive rocks and lavas are very small or negligible.

4. APPLICATION OF OBSERVATION DATA

4.1 Studied Area

The studied area is Yuzawa-Kurikoma area located between the southeastern part of Akita Prefecture and the northwestern part of Miyagi prefecture, Tohoku district of northeast Japan. The area covers approximately 20 km of east-west and 16 km of north-south. The series of volcano are situated in the center of the area. Two geothermal power plants are in operation, namely Uenotai PP own by Tohoku Electric and Wasabizawa PP own by Yuzawa Geothermal.

4.2 Data

The Japan Oil, Gas and Metals National Corporation (JOGMEC) are conducting the series of helicopter airborne geophysical surveys for the purpose of assessment of geothermal resources potential in Japan since 2014. These includes the HeliFALCON™ Airborne Gravity Gradiometer Survey and the HELITEM time domain ElectroMagnetic Survey conducted over the studied area in 2015 whose report and data are provided by JOGMEC (2015).

For the gravity gradiometer survey, the measurement interval is 3m. The line spacing is approximately either 125m or 250m for the east-west lines and 2.5 kms for the north-south lines, respectively. The flight height is designed at 125m.

DEM (10m mesh data) of the Geospatial Information Authority of Japan (GSI (2015)) are publicly obtained.

The coordinate system is based on the zone 10 of the plane rectangular coordinate system whose origin is at latitude 40N and longitude 140.833E.

The observed data sets of both the horizontal gravity-gradient (G_{uv} and G_{xy}) and the total field magnetic intensity anomaly are gridded through a Kriging geostatistical gridding method into the data of 25m interval. The DEM (10m mesh) data are also gridded into the 25m grid data.

4.3 Conventional Analysis

Figure 4 shows the maps of DEM (left) and G_{zz} (right). The vertical gravity-gradient data (G_{zz}) are calculated using the grid data sets of observed horizontal gravity-gradient data (G_{uv} and G_{xy}). Two maps are very similar in shape. This is due to the facts; the explorable depth of the survey is shallow and the data are highly affected by the roughness of the surface (surface effects).

The RTPM data sets are calculated using the grid data sets of observed total field magnetic intensity. The assumption of magnetic inclination is 53 degrees downward and that of declination is 8.1 degrees westward.

The moving window Poisson's analysis is applied for the RTPM data sets and the G_{zz} data sets to produce the $\Delta J/\Delta\rho$ ratio. The size of window is 5 x 5 grids. The result at each grid (x, y) whose correlation coefficient exceed 70% is selected to form the data sets of $\Delta J/\Delta\rho$ ratio.

Figure 5 shows the maps of RTPM (left) and $\Delta J/\Delta\rho$ ratio (right). Two map are similar, however more precise distribution near the locations of volcano is achieved in the map of $\Delta J/\Delta\rho$ ratio, such as positive parallel distribution feature (please see Figure 8 and the Category 3 map of Figure 6). More uniformity is observed outside of volcanic areas. The $\Delta J/\Delta\rho$ ratio is therefore verified to be more indicative parameter which represents the subsurface average magnetization.

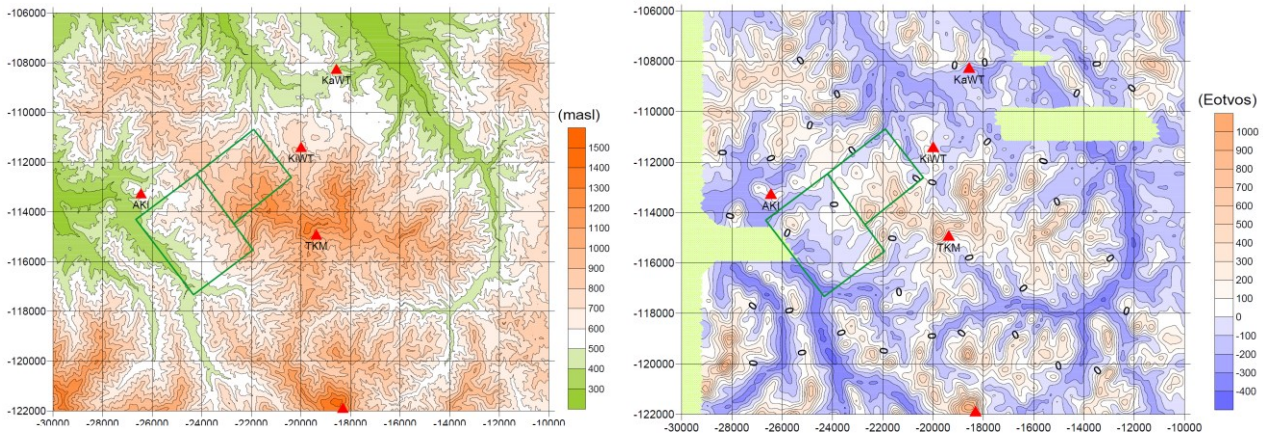

Figure 4: Map of DEM (left) and G_{zz} (right)

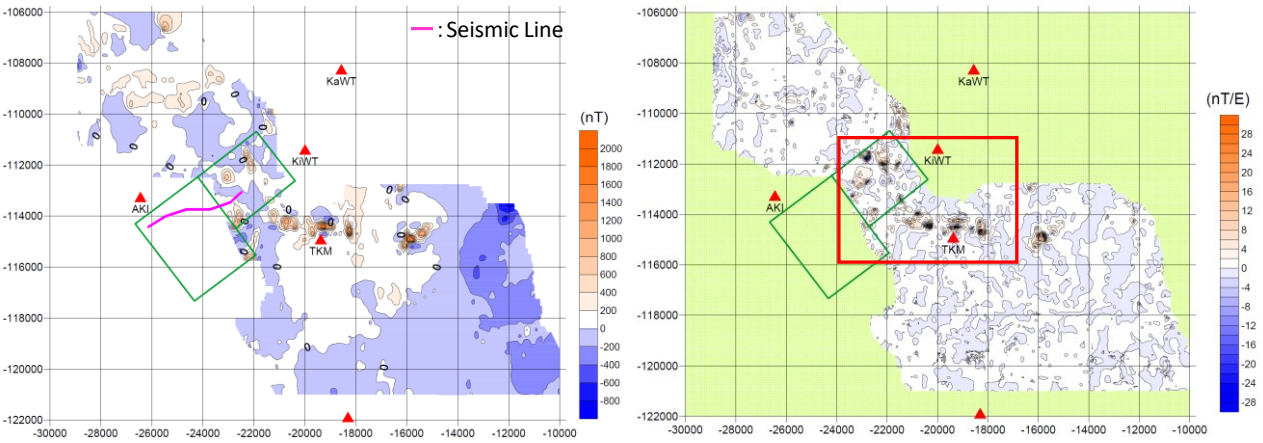

Figure 5: Maps of RTPM (left) and $\Delta J/\Delta\rho$ ratio (right)

4.4 Precise Analysis

Precise analysis of the distribution of $\Delta J/\Delta\rho$ ratio is made in the volcanic area, covering 7 km of east-west and 5 km of north-south as shown as a red rectangular in the right map of Figure 5. The series of volcano are situated in the center of the area, namely from west to east Yamabushi-dake (YBD), Takamatsu-dake (TMD), Ishigami-yama (IKY) and Futtuki-dake (FTD).

Each grid (x,y) is classified into 3 categories depending on the absolute value of $\Delta J/\Delta\rho$ ratio. The absolute value of $\Delta J/\Delta\rho$ ratio in the category 1 is less than 0.42 nT/Eotvos. That in the category 3 is more than 2 nT/Eotvos, while that in the category 2 is in between.

Figure 6 shows the cross-plot (G_{zz}(Eotvos) in y-axis and RTPM(nT) in x-axis) (left) and the map of $\Delta J/\Delta\rho$ ratio (right). Three pairs of these maps are from up to down, those of the category 1, 2 and 3. Only pairs included in each category are used for the cross-plot of such category, and if the $\Delta J/\Delta\rho$ ratio is positive, then such pair's plot is pasted in pink, while negative in blue. In the map of $\Delta J/\Delta\rho$ ratio, the same procedure is applied on each grid. Each grid at which the $\Delta J/\Delta\rho$ ratio is out of such category is blank in white. The grid pasted in light green indicates that there is no geomagnetic data.

Category 1; the areas of low $\Delta J/\Delta\rho$ ratio whose dominant slope is 0.42 nT/E, indicating the areas almost free from magnetized rocks and situated away from volcanic areas. Random distribution of cross-plot reflecting sensitive nature of G_{zz} of the surface effects.

Category 2; the areas of moderate $\Delta J/\Delta\rho$ ratio whose dominant slope is 0.78 nT/E, indicating the areas of lava deposits, horizontal intrusive rocks, deeply seated vertical intrusive rocks or distinctive low-density layers if magnetization is normal.

Category 3; the areas of high $\Delta J/\Delta\rho$ ratio whose dominant slope is 2.7 nT/E, indicating the areas of volcano, vertical intrusive rocks. Vertical intrusive rocks or conduit as shown in pink and surrounding sinking areas as shown in blue if magnetization is normal.

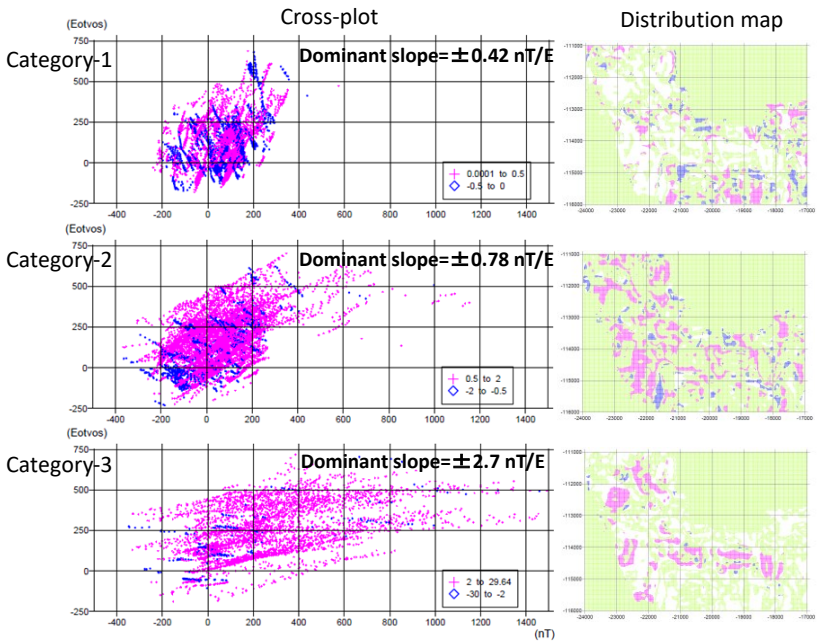

Figure 6: Maps of cross-plot (left) and $\Delta J/\Delta\rho$ ratio (right) for respective categories 1-3.

4.5 Geological model

The studied area is located under the east-west compressional stress fields by the Pacific plate. Figure 7 shows four types of the geological model in view of subsurface magnetized rocks and their geomagnetic responses; vertical intrusion model (VI), two horizontal intrusion models (HI-1 and HI-2) and lava deposit model (LD).

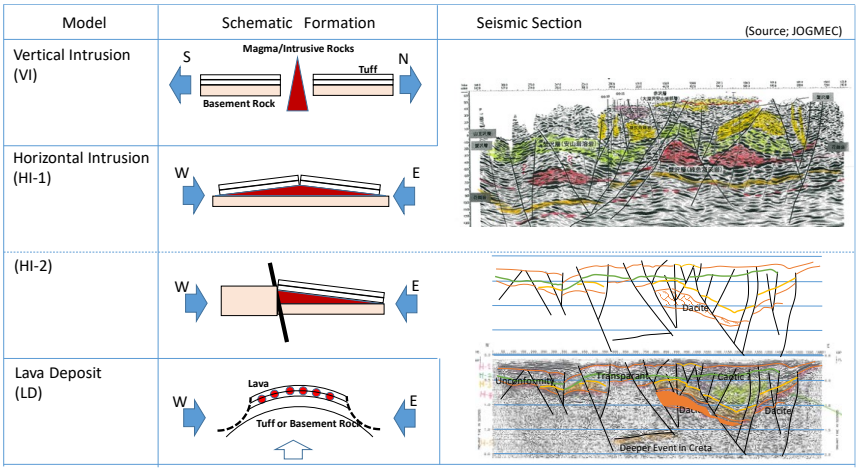

Figure 7: Geological Model

The VI model deals with the vertical intrusion under the north-south expansional stresses. The normal faults will be formed in the east-west direction and may be expected to act as geothermal reservoirs.

The HI-1 and HI-2 models deal with horizontal intrusion under the north-south compressional stresses. The direction of intrusion will be north-south. The intrusion will most probably occur at such boundary separating the over-laid and under-lying rocks whose properties are different, as between tuffs and basement rocks. The convex of over-laid rock such as tuff may be fractured and may form small geothermal reservoirs. The difference of HI-1 and HI-2 is the rocks of both sides of the fault. The former is the same type of rocks while the latter is different (tuff and basement rocks encountering basement rocks only). These phenomena can be observed in the seismic sections acquired by JOGMEC. The upper section is shown as an example of HI-1 acquired around the area of Onikobe geothermal PP about 20 km south-east of the studied area, while the lower one is shown as an example of HI-2 acquired around the area of Yamakawa geothermal PP in Kyushuu. The faults are supposed to act as feeding passes of magma underlain.

The LD model deals with massive lava deposits on tuff and/or basement rocks. The upheaval, whose direction will be north-south will be formed under the east-west compressional stresses. And the concave portion will be subject to erosion by the streams etc., while that of convex remains which gives geo-magnetic effects.

4.6 Geological Interpretation

The Figure 8 shows the interpretation of the linearity of the distribution of ΔJ/Δρ ratio (left) and its comparison with the geological map (right). The linearity of large values of ΔJ/Δρ ratio is the basis of interpretation. The linear lines are drawn on the distribution map of ΔJ/Δρ ratio to produce the left map. The interpreted lines are also drawn on the geological map provided by the geological survey of Japan (GSJ) (2015), which shows the areas of lava deposits and major faults, Wasabizawa and Doroyu. The arrows in the maps is the interpreted direction of stresses.

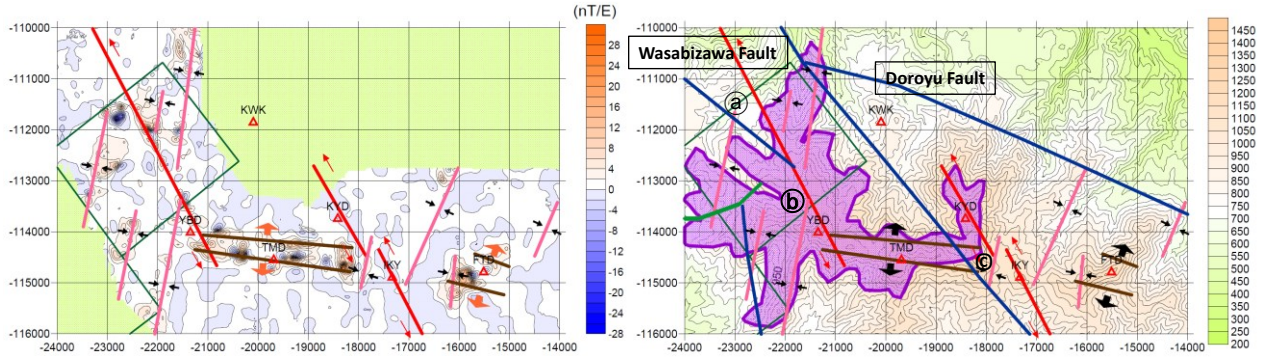

Figure 8: Interpretation

Two left-lateral strike-slip faults (shown in red line) whose direction is northwest-southeast are interpreted; one passing through the YBD, another passing through the IKY-KYD and possibly extending to Kawarage fumarole (KWK). The latter may be considered as echelon fault and form small pull apart basins along the fault such as at (c), inducing possible intermittent releasing fractures.

Two normal faults (shown in brown line) whose direction is in east-west are interpreted; one is large encompassing about 3 km centered at the TMD and passing towards the west at the YBD, another is small at the FTD. Parallel feature of high ΔJ/Δρ ratio associated with that of low in between indicates the formation of small pair of normal faults and the presence of cracks with low-density in between. Each fault may induce possible continuous releasing fractures and be expected to act as geothermal reservoirs.

Several north-south to NNE-SSE linearities of the distribution of ΔJ/Δρ ratio (shown in pink line) are observed. Five of them are appeared in the western part. They are situated on the areas of lava deposits. As the underlain magma need to be provided vertically through such openings as the ones developed along the strike-slip faults to form the horizontal intrusion, it is unlikely to correspond to the types of HI-1 or HI-2, if the interpreted linearities do not reach to the fault. Therefore, two of them are considered as the type of LD (one of them, see at (a)). Other three need to be further analysis (one of them, see (b)), however they follow the trend of lava deposits, and are likely to be the type of LD. In the eastern part, four linearities are situated at out of the areas of lava deposit. They are of small size. Three of them reach to or straddle on the strike-slip faults. They may be corresponding to the type HI-1 or HI-2 and induce possible releasing fracture and be expected to act as small geothermal reservoirs.

5. CONCLUSION

Airborne geophysical surveys acquired at low flight height close to the ground are the speedy, effective and cost saving method to evaluate the geothermal resources potential. The two-dimensional analysis can be achieved with such fine grid interval as 25m. The integrated analysis of gravity-gradient and geomagnetic survey data applying the moving window Poisson's analysis will lead to the assessment of the detailed near-surface magnetization-to-density ratio. The application of the observation data is enough satisfactory. The correlation between the two data sets are quite good. The areas of its high values are related to the ones where massive magnetized rocks are present. These are not only appeared to surface but also buried volcanic conduits and dikes, buried horizontal intrusive rocks, massive lava deposits etc. The hidden strike-slip faults are properly interpreted using the linearity of magnetization-to-density ratio and the regional compressional stress fields are verified to be active in the studied area. The normal faults can be delineated which are formed under the local expansional stress fields which are orthogonal to the regional compressional stress fields. The results obtained through the analysis helps to understand the subsurface geology and contribute to the assessment of the heat sources and reservoirs of geothermal resources. It may be more beneficial to combine further with the estimation of low-density areas of surface-layer through the HGGS analysis of the gravity-gradient data for obtaining the better images of subsurface geo-circulation system of geothermal fluid.

REFERENCES

Chandler, V. W., J. S. Koski, W. J. Hinze and L. W. Braile: Analysis of multi-source gravity and magnetic anomaly data sets by moving-window application of Poisson's theorem, Geophysics, 46, (1981), 30-39.

Geological Survey of Japan, AIST: Seamless digital geological map of Japan 1:200,000 May 29 2015 version, National Institute of Advanced Industrial Science and Technology, (2016).

Geospatial Information Authority of Japan, GSI: Numerical Elevation Model 10m mesh, Foundation Map Download Service, (2015).

Hancock, P.L.: Continental Deformation, Pergamon Press, (1994), 421p.

JOGMEC: HeliFALCONTM Airborne Gravity Gradiometer Survey Kujyu and Kirishima, Kyushu Japan Logistics and Processing Report, JOGMEC Report, (2014).

JOGMEC: The fiscal year 2015 Airborne Geophysical Survey for the Geothermal Resources Potential Report (in Japanese), JOGMEC Report, (2015).

Mizutani, Shigeki: The Correlation between Seismic and Logging Data and Its Geological Interpretation in the Akinomiya/Wasabizawa Geothermal Area, Journal of the Geothermal Research Society of Japan, 34, No.1 (2012), 21-35 (abstract and figures in English, text in Japanese).

Mizutani, Shigeki: The trial of integrated analysis of gravity and geomagnetic data for geothermal resource evaluation, Journal of the Geothermal Research Society of Japan, 38, No.3 (2016), 71-84 (abstract and figures in English, text in Japanese).

Mizutani, Shigeki: A new approach of estimating density variations of surface-layers using horizontal gravity gradient data, Proceedings, 13th SEGJ International Symposium, (2018).

Poisson, S.D.: Memoire sur la theorie du magnetism, Memoires de l'Academie Royale des Sciences de l'Institut de France, (1826), 247-348.

Taira, Asahiko: Interpretation of Geological Layers, Geology Volume 2, Iwanami Press, (2001), 441p.